Acta Crystallographica Section D
Biological Crystallography
ISSN 0907-4449

Structures of the ribosome-inactivating protein from barley seeds reveal a unique activation mechanism

Byung-Gil Lee,[a] Min Kyung Kim,[a] Byeong-Won Kim,[a] Se Won Suh[b,c] and Hyun Kyu Song[a]*

[a]School of Life Sciences and Biotechnology, Korea University, Seoul 136-701, Republic of Korea, [b]Department of Chemistry, College of Natural Sciences, Seoul National University, Seoul 151-747, Republic of Korea, and [c]Department of Biophysics and Chemical Biology, College of Natural Sciences, Seoul National University, Seoul 151-742, Republic of Korea

Correspondence e-mail: hksong@korea.ac.kr

Received 25 June 2012
Accepted 28 August 2012

PDB References: barley RIP, 4fb9; 4fba; 4fbb; 4fbc; 4fbh

Ribosome-inactivating protein (RIP), a defence protein found in various plants, possesses different chain architectures and activation mechanisms. The RIP from barley (bRIP) is a type I RIP and has sequence features that are divergent from those of type I and type II RIPs from dicotyledonous plants and even the type III RIP from maize. This study presents the first crystal structure of an RIP from a cereal crop, barley, in free, AMP-bound and adenine-bound states. For phasing, a codon-optimized synthetic *brip1* gene was used and a vector was constructed to overexpress soluble bRIP fusion proteins; such expression has been verified in a number of cases. The overall structure of bRIP shows folding similar to that observed in other RIPs but also shows significant differences in specific regions, particularly in a switch region that undergoes a structural transition between a 3_{10}-helix and a loop depending on the liganded state. The switch region is in a position equivalent to that of a proteolytically susceptible and putative ribosome-binding site in type III RIPs. Thus, the bRIP structure confirms the detailed enzymatic mechanism of this N-glycosidase and reveals a novel activation mechanism for type I RIPs from cereal crops.

1. Introduction

Ribosome-inactivating proteins (RIPs) are widely distributed in the plant kingdom and play a critical role in defence against pathogens (Gould & Richardson, 1987; Peumans *et al.*, 2001; Van Damme *et al.*, 2001). Their physiological function is the inhibition of protein synthesis by damaging the ribosomes of the pathogen *via* cleavage of the N-glycosidic bond of an adenine located in the α-sacrin/ricin loop in ribosomal RNA (Endo & Tsurugi, 1987). This depurination prevents the binding of elongation factors to the ribosome or aminoacyl-tRNA and induces cell death (Stirpe, 2004; Stirpe & Battelli, 2006). Besides depurinating rRNA, RIPs are also known to release adenine bases from various DNAs, capped mRNAs and poly(A) strands, and have RNAse and DNAse activity (Peumans *et al.*, 2001).

RIPs have been classified into three groups depending on their physical properties (Nielsen & Boston, 2001). Type I RIPs are monomeric single-chain enzymes with N-glycosidase activity, and most RIPs, including trichosanthin (TCS) and pokeweed antiviral protein (PAP), belong to this class. Type II RIPs, such as ricin and abrin, are larger heterodimeric proteins that consist of an enzymatic A-chain and a lectin-binding B-chain. The A-chain, which has N-glycosidase activity, resembles type I RIPs and is connected to the B-chain by a disulfide bond. Type II RIPs, unlike type I RIPs, are usually

highly toxic to intact cells owing to the presence of the lectin-binding B-chain, which binds to cell-surface receptors that contain terminal galactose sugar residues (Bieri *et al.*, 2000; Stirpe & Battelli, 2006; Stirpe *et al.*, 1986). Type III RIPs, such as maize b-32 and barley JIP60, are unusual RIPs (Chaudhry *et al.*, 1994). They are synthesized as inactive precursors in the cytoplasm and are activated by the proteolytic removal of peptide fragments; the structures of activated type III RIPs are known to resemble those of type I RIPs (Mak *et al.*, 2007; Yang *et al.*, 2010).

RIPs have attracted considerable interest in recent years because of their potential applications in agriculture and medicine. In agriculture, some RIPs such as barley RIP, PAP, TCS and dianthin have been observed to increase resistance towards viruses, fungi and other possible pathogens (Parikh & Tumer, 2004; Lodge *et al.*, 1993). In medicine, they have been studied as potential immunotoxins that can be selectively targeted to a particular cell type such as cancer cells (Vitetta & Uhr, 1985; Pastan & Kreitman, 1998; Bolognesi & Polito, 2004; Polito *et al.*, 2011). Type I RIPs are thought to be better candidates than type II or type III RIPs for the construction of immunotoxins because they lack their own cell-recognition and binding ability and need no additional proteolytic step. The toxicity of type I RIPs can be greatly enhanced by coupling them to a cell-binding protein (such as an antibody or lectin) or by incorporating them into liposomes or erythrocyte ghosts, which can fuse with intact cells (Provoda *et al.*, 2003). Moreover, some type I RIPs have also been shown to have potent activity against HIV-1-infected T cells and macrophages (McGrath *et al.*, 1989; Lee-Huang *et al.*, 1990).

Crystal and solution structures of RIPs from diverse species have been reported (Robertus & Monzingo, 2004; Gorjanović, 2009) and a list of representative structures follows. (i) Type I RIPs: PAP (Monzingo *et al.*, 1993), TCS (Zhou *et al.*, 1994) and charybdin (Touloupakis *et al.*, 2006). (ii) Type II RIPs: ricin (Montfort *et al.*, 1987) and abrin (Tahirov *et al.*, 1995). (iii) Type III RIP: maize b-32 (Mak *et al.*, 2007; Yang *et al.*, 2010). These structures show that all three types of RIPs share a similar folding pattern and active-site structure; however, each structure also has unique features. Although a vast amount of structural information is available on RIPs from diverse plant species, relatively limited information is available on those from monocotyledonous plants.

RIPs isolated from barley (*Hordeum vulgare* L.) seeds were among the first identified RIP enzymes (Asano *et al.*, 1984; Motto & Lupotto, 2004) and are the most well characterized RIPs from a cereal crop (Asano *et al.*, 1986; Endo *et al.*, 1988; Leah *et al.*, 1991). They consist of two isoforms, RIP30 and RIP30A (named RIP1 and RIP2, respectively, in barley), with a sequence identity of 97%. They belong to the type I category and inactivate eukaryotic ribosomes *via* a mechanism identical to that of the ricin A-chain, *i.e.* by hydrolyzing the N-glycosidic bond at adenine 4324 of the 28S rRNA of the eukaryotic 60S ribosomal subunit (Endo *et al.*, 1988). They have also been reported to exhibit antifungal activity (Roberts & Selitrennikoff, 1986). The sequences of barley RIP1s have more than 50% identity to those of type I RIPs from cereal crops (Fig. 1). However, they have a sequence homology of less than 30% to structurally characterized RIPs, including monocot RIPs such as charybdin and maize RIP.

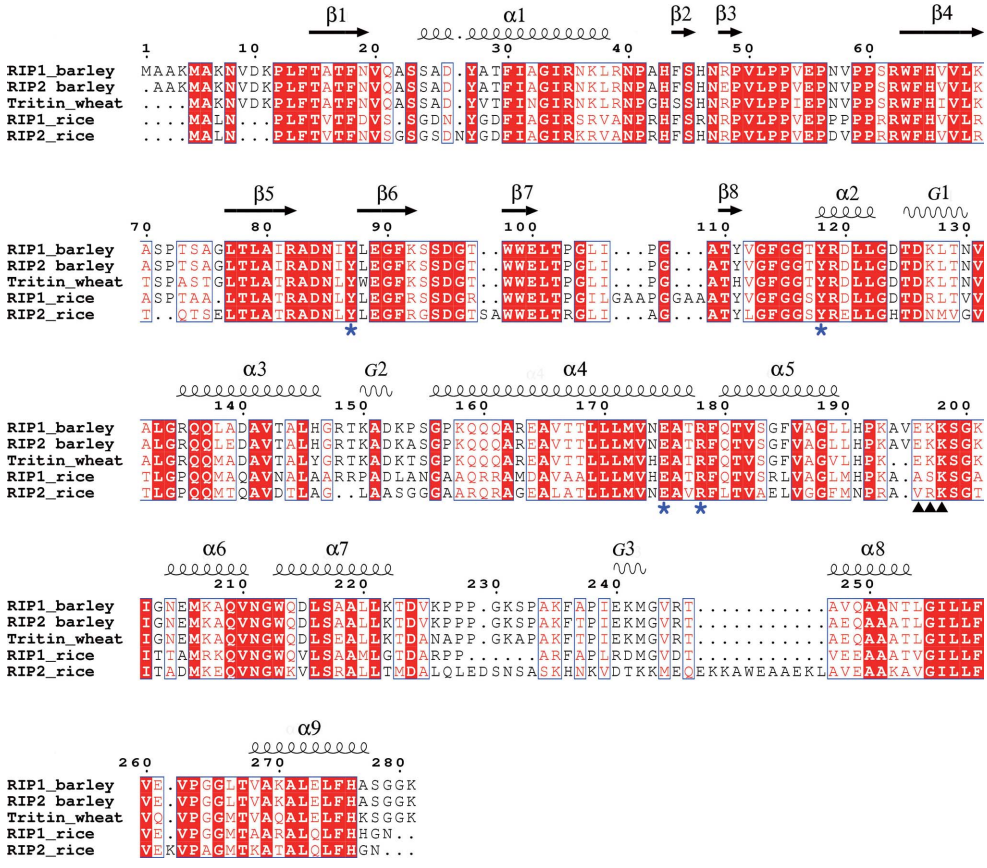

Figure 1
Structure-based sequence alignment of RIPs from several cereal crops. Completely conserved residues are represented as white letters on a red background and highly conserved residues are represented as red letters. The sequence identity of RIP1_barley (bRIP) to RIP2_barley, tritin_wheat, RIP1_rice and RIP2_rice is 97, 89, 65 and 54%, respectively. The catalytic residues in the active site are marked by asterisks. The mutated residues for SER are marked by filled black triangles. The secondary-structural elements of bRIP are indicated above the sequence (α-helices, springs; β-strands, black arrows; 3_{10}-helices, wavy lines). The alignment was generated using *ClustalW* and *ESPript* (Larkin *et al.*, 2007; Gouet *et al.*, 1999).

In this study, we report the crystal structures of barley RIP1 (bRIP) in the free form as well as in complex with AMP and adenine. Although we previously obtained X-ray-diffracting crystals of bRIP isolated from natural sources (Song *et al.*, 1994), it took a very long time to overcome phase-related issues. The details of the structure determination are described here. Our study of bRIP provides information on the unique structural features of RIPs from cereal crops, which differ from those of other RIPs.

2. Materials and methods

2.1. Sample preparation

bRIP extracted from natural barley seeds was purified by ammonium sulfate precipitation, cation-exchange and size-exclusion chromatography as detailed in a previous report (Song *et al.*, 1994). The codon-optimized *H. vulgare* L. *rip1* gene was purchased from Cosmo Genetech, Seoul, Republic of Korea. The *brip1* gene was cloned into a modified pET vector (pET-His) containing a tobacco etch virus (TEV) protease cleavage site preceded by an amino-terminal six-histidine tag. The $bRIP_{SER}$ mutant (E196A/K197A/K198A) was designed using the *SERp* (*Surface Entropy Reduction prediction*) server (http://nihserver.mbi.ucla.edu/SER/; Goldschmidt *et al.*, 2007) and generated using the QuikChange site-directed mutagenesis method (Stratagene, La Jolla, California, USA). The cloned vector was transformed into *Escherichia coli* BL21 (DE3) cells. Expression of $bRIP_{SER}$ was induced by the addition of 1 m*M* IPTG at an OD (at 600 nm) of 0.5. The harvested cells were resuspended in buffer *A* (50 m*M* Tris–HCl pH 8.0, 100 m*M* NaCl) and disrupted by ultrasonication. The cell lysate was clarified by centrifugation and applied onto a HisTrap Ni–NTA column (GE Healthcare). TEV protease was added to the eluent in order to cleave the histidine affinity tag and the cleavage products were further purified using a HiTrap Blue column (GE Healthcare) and a Superdex 75 GL gel-filtration column (GE Healthcare). The purified $bRIP_{SER}$ protein was concentrated to 40 mg ml^{-1} in storage buffer (buffer *A* with 2 m*M* DTT). Selenomethionyl (SeMet) $bRIP1_{SER}$ protein was expressed in the methionine auxotroph *E. coli* B834 (DE3) in minimal medium containing selenomethionine and was purified using the same protocol as used for native $bRIP_{SER}$.

Another vector (designated here as pET-RIP) was generated with the aim of producing soluble fusion protein by inserting the *brip1* gene into the site between the amino-terminus and the TEV protease-cleavage site of the pET-His vector (Fig. 2*a*) using enzyme-free (EF) cloning methods (Tillett & Neilan, 1999) with eight primers (purchased from IDT). We cloned the PCR-amplified *yjbH* and *sepF* genes from *Bacillus subtilis*, the ClpS-homology domain of the human *ubr1* gene and a fragment of the *atg1* gene from yeast into the pET-RIP vector, transformed them into *E. coli* BL21 (DE3) cells and induced their expression by the addition of 1 m*M* IPTG. Cells were separated into soluble and pellet fractions by centrifugation. The expression and solubility of the proteins were evaluated using SDS–PAGE (Figs. 2*b*–2*e*).

2.2. Crystallization and data collection

All crystallizations were performed using the hanging-drop vapour-diffusion method at 295 K. Crystals of AMP-bound bRIP were obtained by AMP cocrystallization using the following reservoir conditions: 100 m*M* Tris–HCl pH 8.41, 27.5%(*w*/*v*) polyethylene glycol 1500. X-ray data were collected from a single crystal at 290 K using the laboratory X-ray system. Detailed methods for the crystallization and data collection of bRIP have been described in a previous report (Song *et al.*, 1994).

Crystals of $bRIP_{SER}$ were obtained using a reservoir solution consisting of 100 m*M* phosphate–citrate pH 4.2, 200 m*M* sodium chloride, 20%(*w*/*v*) polyethylene glycol 8000. Cocrystallization and soaking were performed to obtain crystals of bRIP in complex with adenine and AMP. For cocrystallization, an approximately threefold molar excess of AMP was added to $bRIP_{SER}$ and incubated for 24 h at 277 K; crystals could be obtained under these conditions. For soaking with adenine and AMP, an ∼12-fold molar excess of a solution of adenine and AMP was applied to pre-grown $bRIP_{SER}$ crystals and incubated for 24 h. Crystals of SeMet $bRIP_{SER}$ were obtained with 100 m*M* MES pH 6.0, 200 m*M* calcium acetate, 20%(*w*/*v*) polyethylene glycol 8000. For cryo experiments, crystals were transferred to reservoir solution containing 20%(*w*/*v*) glycerol before flash-cooling in a nitrogen stream at 100 K. X-ray data were collected on the 17A and NW12 beamlines at the Photon Factory (PF), Japan. The diffraction data were processed using *HKL*-2000 (Otwinowski & Minor, 1997).

2.3. Structure determination and refinement

Initial phases for SeMet $bRIP_{SER}$ were obtained by *Phaser* using the single-wavelength anomalous dispersion (SAD) method (McCoy *et al.*, 2007). The initial model was automatically constructed using *Buccaneer* (Cowtan, 2006). Further model building was performed using *Coot* (Emsley *et al.*, 2010). The protein model was refined using *REFMAC* (Murshudov *et al.*, 2011) and *PHENIX* (Adams *et al.*, 2010). The phases of adenine-bound and AMP-bound $bRIP_{SER}$ and bRIP were obtained by molecular replacement using *MOLREP* (Vagin & Teplyakov, 2010) and *Phaser* (McCoy *et al.*, 2007) with the refined $bRIP_{SER}$ as a search model. The positions of the adenine and AMP were determined using an $F_o - F_c$ difference Fourier map contoured at 2.5σ. The final refinement and validation of all models were obtained using *PHENIX* (Adams *et al.*, 2010) and *PROCHECK* (Laskowski *et al.*, 1993). The *DALI* server (Holm & Rosenström, 2010; http://ekhidna.biocenter.helsinki.fi/dali_server/) was used for structural comparisons. Data-collection, phasing and refinement statistics are summarized in Table 1. All structural figures in this article were prepared using *PyMOL* (http://www.pymol.org/).

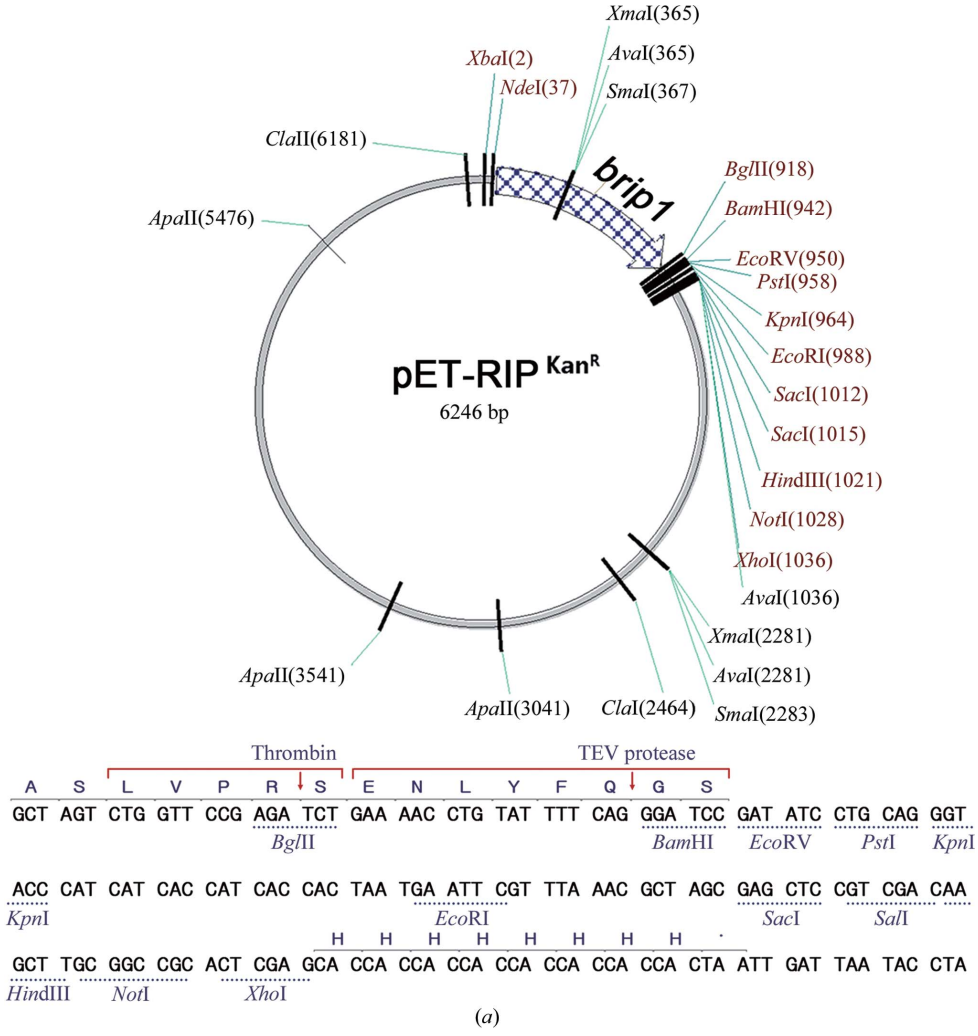

(*a*)

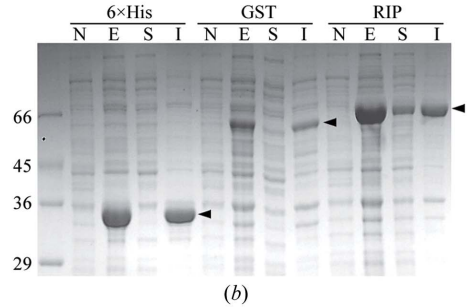

(*b*)

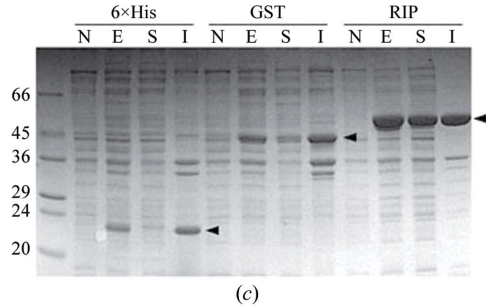

(*c*)

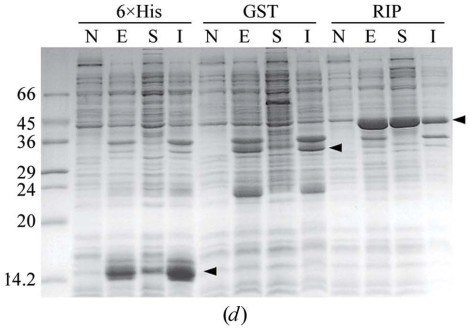

(*d*)

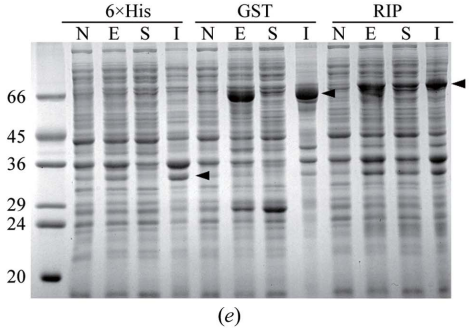

(*e*)

3. Results and discussion

3.1. Existing problems in structure determination of bRIP

We have previously extracted and purified the bRIP protein from natural barley seeds and crystallized the protein in complex with AMP (Song *et al.*, 1994). The crystals belonged to space group *C*2, with one monomer in each asymmetric unit. Initially, we tried to solve the structure by using the molecular-replacement technique, as several RIP structures, including those of ricin, momorcharin, TCS and PAP, were available at the time. These RIPs were obtained from dicotyledonous plants and showed approximately 20% sequence identity to bRIP, suggesting the presence of structural differences in several regions. Subsequently, the coordinates of monocotyledonous RIPs such as b-32 from maize and charybdin became available; however, we failed to obtain

Figure 2
Overexpression of the bRIP-fusion protein. (*a*) Expression vector for the bRIP-fusion protein. The synthetic codon-optimized *brip1* gene was inserted into the modified pET vector (Novagen) containing six histidine residues at the N-terminus. Immediately after the bRIP-coding sequence are the thrombin and TEV protease cleavage sites. Therefore, the translated product is as follows: MHHHHHH-(bRIP)-ASLVPRSENLYFQGS-(target protein). Multiple cloning sites are observed starting from the *Bgl*II recognition sequence (918) and eight noncleavable C-terminal histidine residues can be attached to the target protein depending on the construct design. (*b*–*e*) Expression and solubility tests of the bRIP-fusion proteins YjbH (*b*) and SepF (*c*) from *B. subtilis*, ClpS-homology domain of human Ubr1 (*d*) and a fragment of Atg1 from yeast (*e*). 6×His, GST and RIP indicate the N-terminal six-His tag, the GST-fusion protein and bRIP, respectively. The proteins expressed are marked with black filled arrowheads. N, non-induced total cell extract; E, expressed total cell extract; S, soluble fraction; I, insoluble fraction.

Table 1
Data-collection and refinement statistics.

Values in parentheses are for the highest resolution shell.

	Native	SER†			
	AMP cocrystal	Apo form (SeMet-labelled)	Adenine-soaked	AMP cocrystal	AMP-soaked
Data-collection statistics					
Space group	*C*2	*C*2	*C*2	*C*2	*C*2
X-ray source	Cu *Kα*	17A, PF	17A, PF	NW12, PF	17A, PF
No. of molecules in asymmetric unit	1	4	4	4	4
Unit-cell parameters (Å, °)	*a* = 88.36, *b* = 62.59, *c* = 53.18, *α* = *γ* = 90, *β* = 108.62	*a* = 130.3, *b* = 142.9, *c* = 84.8, *α* = *γ* = 90, *β* = 126.9	*a* = 131.0, *b* = 142.4, *c* = 85.8, *α* = *γ* = 90, *β* = 127.5	*a* = 131.3, *b* = 142.5, *c* = 85.1, *α* = *γ* = 90, *β* = 127.5	*a* = 133.8, *b* = 142.4, *c* = 85.2, *α* = *γ* = 90, *β* = 128.0
Wavelength (Å)	1.5418	0.97913 [peak]	1.0000	1.0000	1.0000
Resolution (Å)	2.3 (2.60–2.30)	1.75 (1.81–1.75)	1.85 (1.92–1.85)	1.8 (1.83–1.80)	1.7 (1.76–1.70)
$R_{\rm merge}$‡ (%)	5.3	8.4 (49.1)	6.9 (44.0)	3.9 (33.8)	5.3 (46.4)
Average $I/\sigma(I)$	69.8 (19.6)	17.6 (2.1)	24.2 (2.5)	40.1 (5.1)	26.0 (1.9)
Completeness (%)	89.5 (80.4)	99.2 (98.6)	96.8 (93.7)	99.6 (99.0)	98.0 (96.4)
Multiplicity	3.75	3.6 (3.1)	3.8 (3.5)	4.2 (3.9)	3.8 (3.5)
Refinement statistics					
Resolution (Å)	25.5–2.3	41.3–1.75	47.6–1.85	31.5–1.8	37.7–1.7
No. of reflections	11803	123236	94861	113733	134038
$R_{\rm work}/R_{\rm free}$§ (%)	17.8/24.4	17.1/19.7	17.1/20.2	21.0/25.0	17.6/21.4
No. of atoms					
Protein	2018	8346	8364	8328	8333
Ligand/ion	23 [AMP]		40 [adenine]	30 [adenine]	92 [AMP]
Water	92	1822	1362	1247	1970
Average *B* factors (Å^2)					
Protein	31.9	16.6	25.3	28.5	21.6
Ligand/ion	35.4 [AMP]		22.3 [adenine]	29.6 [adenine]	35.1 [AMP]
Water	35.0	26.0	34.0	32.1	31.6
R.m.s. deviations					
Bond lengths (Å)	0.007	0.007	0.007	0.007	0.007
Bond angle (°)	1.107	1.072	0.977	1.065	1.087
Ramachandran plot					
Most favoured (%)	96.8	94.4	95.0	94.6	94.7
Additionally allowed (%)	3.2	5.2	5.0	5.4	5.3
Generously allowed (%)	0	0	0	0.1	0
Disallowed (%)	0	0	0	0	0
PDB code	4fbh	4fb9	4fba	4fbb	4fbc

† Surface-entropy reduction (triple mutant, E196A/K197A/K198A). ‡ $R_{\rm merge} = \sum_{hkl}\sum_i |I_i(hkl) - \langle I(hkl)\rangle|/\sum_{hkl}\sum_i I_i(hkl)$, where $I_i(hkl)$ is the intensity of the *i*th measurement of *hkl* and $\langle I(hkl)\rangle$ is the corresponding average value for all *i* measurements. § $R_{\rm work} = \sum_{hkl}||F_{\rm obs}| - |F_{\rm calc}||/\sum_{hkl}|F_{\rm obs}|$; $R_{\rm free}$ was calculated using 5% of the data.

phases owing to the relatively low sequence identity (∼30%). Next, we tried to screen heavy-atom derivatives to obtain phases by using the multiple isomorphous replacement method. No heavy-metal derivative could be obtained, probably owing to the lack of free cysteine residues in bRIP (Fig. 1). Considering the structure of the ricin A-chain, crystallization of bRIP was performed in the presence of 2-bromoadenine in order to obtain phases by locating the Br atom in the crystal. Unfortunately, bRIP could not be crystallized in the presence of the halogen-derivatized adenine.

Another problem that was encountered was related to purification and crystallization. Although we obtained diffracting crystals of bRIP (Song *et al.*, 1994), the protein purification yields varied with different batches of barley seeds and subsequently the crystallization was not reproducible. We further tried reductive methylation of the surface lysine residues, as it has been reported that introduction of a hydrophobic methyl moiety can improve crystallization and diffraction quality (Rayment, 1997). Methylated bRIP has been crystallized, but only needle-shaped crystals were obtained. Inevitably, we needed the *brip1* gene for heterologous bacterial expression to apply MAD phasing. Bacterial expression of several RIPs has been reported (Mlsna *et al.*, 1993); however, only very limited success has been achieved in the recombinant expression of RIP genes from cereal crops such as wheat and rice (Bieri *et al.*, 2000). Although cloning of the *brip1* gene has previously been reported (Leah *et al.*, 1991), the lack of soluble overexpression of the protein may also hinder structural studies.

3.2. Overexpression of bRIP and its application

In recent years, the synthesis of entirely codon-optimized genes has become very robust and is extremely useful for obtaining large quantities of protein samples for X-ray studies (Jeong *et al.*, 2011). The codon-optimized *rip1* gene from barley was synthesized with *Bam*HI and *Hin*dIII restriction enzyme sites at the 5′ and 3′ ends, respectively. It was ligated into a modified pET vector (see §2), with its expression under the control of IPTG. The bRIP protein is overexpressed in

E. coli and is exceptionally soluble. Standard purification steps including His-tag affinity, HiTrap Blue affinity and size-exclusion chromatography yielded more than 200 mg homogeneous bRIP per litre of culture. Subsequently, we constructed another plasmid, pET-RIP, to express a fusion protein consisting of bRIP at the N-terminal region and a target protein at the C-terminal region (Fig. 2*a*). In our construct, a six-His tag is attached for affinity purification; furthermore, the bRIP protein has a strong affinity for the HiTrap Blue column, facilitating purification. Thrombin and TEV protease sites were inserted into the region between bRIP and the target protein (Fig. 2*a*). We prepared several constructs to demonstrate the efficiency and practicality of this vector, with inserts of variable size as well as from diverse origins: YjbH and SepF from *B. subtilis*, the ClpS-homologous domain of human Ubr1 and a fragment of Atg1 from yeast (Figs. 2*b*–2*e*). These proteins were insoluble when expressed as His-tag or GST-fusion constructs, but were dramatically overexpressed as soluble bRIP-fusion proteins (Figs. 2*b*–2*e*). Therefore, our bRIP-containing vector (pET-RIP) can be used as an alternative to overcome hurdles in the expression, solubilization and purification of other target proteins for structural studies.

3.3. Structure determination and quality of the model

SeMet bRIP was successfully prepared and the yield was approximately 100 mg per litre of bacterial culture at 291 K. However, we still faced problems in obtaining X-ray-diffracting crystals of bRIP. Therefore, we tried another approach for generating good diffracting and reproducible crystals known as the SER method (Cooper *et al.*, 2007; Goldschmidt *et al.*, 2007). A triple mutant, E196A/K197A/K198A, was designed based on the suggestion of the *SERp* server (http://nihserver.mbi.ucla.edu/SER/). The yield of this SER mutant, $bRIP_{SER}$, was approximately 100 mg per litre of bacterial culture and $bRIP_{SER}$ gave well diffracting monoclinic crystals with four molecules per asymmetric unit (Table 1). Coincidentally, the space group (*C*2) was the same as that of a crystal obtained using bRIP from natural barley seeds, but the copy number in the asymmetric unit was different. We also obtained a selenomethionine-substituted crystal of $bRIP_{SER}$ which diffracted to 1.75 Å resolution. The $bRIP_{SER}$ structure was determined by SAD phasing and refined to a crystallographic *R* factor of 0.171 (R_{free} = 0.197). The phase information for bRIP was determined by molecular replacement using the refined $bRIP_{SER}$ model and the structural model of bRIP was refined at 2.3 Å resolution to an *R* factor of 0.178 (R_{free} = 0.244). According to the *PROCHECK* analysis (Laskowski *et al.*, 1993), 100% of the residues of bRIP were located in the most favoured and allowed regions of the Ramachandran plot and no residues were present in the disallowed region (Table 1). Additionally, we generated crystals of $bRIP_{SER}$ with AMP and adenine using both cocrystallization and soaking methods in order to investigate the enzymatic reaction mechanism of bRIP. The crystals of adenine-soaked, AMP-cocrystallized and AMP-soaked $bRIP_{SER}$ diffracted to 1.85, 1.8 and 1.7 Å resolution, respectively, and the final R_{work}/R_{free} values

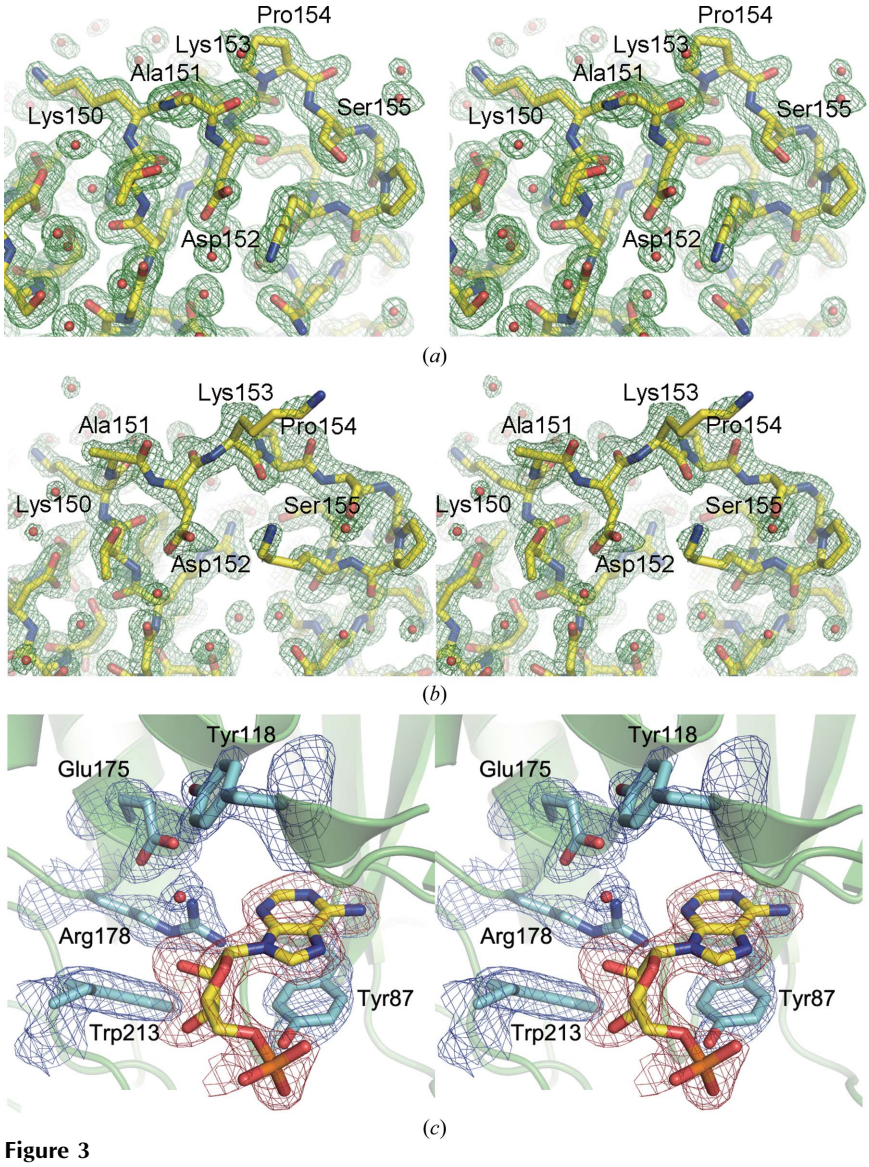

Figure 3
Representative electron-density map. (*a*) A view near 3_{10}-helix G2 (residues Lys150–Lys153) of bRIP. The final $2F_o - F_c$ map (green) was calculated using 41.5–1.75 Å resolution data and was contoured at 1.0σ. (*b*) The same region as in (*a*) in a loop conformation. The final $2F_o - F_c$ map was calculated using 41.5–1.75 Å resolution data and was contoured at 1.0σ. (*c*) A view showing bound AMP. The final $2F_o - F_c$ map for bRIP (blue) and the $F_o - F_c$ OMIT map for AMP (red) were calculated using 25.5–2.3 Å resolution data and were contoured at 1.0σ and 2.5σ, respectively.

after refinement were 0.171/0.202, 0.210/0.250 and 0.176/0.214, respectively. The refinement statistics are shown in Table 1.

3.4. Overall structure of bRIP

In the final model of bRIP, the first three residues, as well as residues 192–197 and 229–233, are not observed in the final electron density and are likely to be unconstructed or flexible. With the exception of these three regions, all residues of bRIP and the bound ligand were well fitted into high-quality electron-density maps (Fig. 3) and no glycosylation sites were detected. The bRIP structure possesses a typical RIP fold (Robertus & Monzingo, 2004) and consists of two separate domains (Fig. 4*a*). The larger N-terminal domain consists of residues 1–211 containing five α-helices (α1–α5), two 3_{10}-helices (G1 and G2), six major β-strands (β1 and β4–β8) and one short pair of antiparallel β-sheets (β2 and β3). The helices and strands alternate in the order β1–α1–β2–β3–β4–β5–β6–β7–β8–α2–G1–α3–G2–α4–α5 (Fig. 4*b*). The first strand β1 and the short strand β8 lie parallel to the neighbouring strands β4 and β7, respectively, and the four central β-strands (β4–β7) are antiparallel (Fig. 4). The smaller C-terminal domain has only five helices containing one 3_{10}-helix (α6–α7–G3–α8–α9). An active-site pocket containing the invariant RIP residues Tyr87, Tyr118, Glu175, Arg178, and Trp213 is formed between the two domains. The electron density of bound AMP was well defined in this active-site pocket (Fig. 3*c*).

All of the residues of bRIP$_{SER}$ except for the first three residues have been built into the electron-density maps. As noted, we introduced three mutations E196A/K197A/K198A for SER; these are located within an invisible loop (residues 192–197) of bRIP (Fig. 4*a*). The other invisible region (residues 229–233) was clearly traced and seems to be ordered by close contact with different crystalline packing regions. There are four molecules of bRIP$_{SER}$ in the asymmetric unit and we first analyzed the root-mean-square deviations (r.m.s.d.s) among these four copies (Fig. 5*a*). The r.m.s.d. was in the range 0.3–0.6 Å, confirming that the independently observed bRIP$_{SER}$ molecules have basically the same structure. However, one region (residues 150–153) showed two different conformations (3_{10}-helix G2 *versus* loop) in one of the four chains (Figs. 5*a* and 5*b*). Furthermore, both the bRIP and bRIP$_{SER}$ structures show essentially the same structure, with an r.m.s.d. of less than 0.9 Å, although a few regions deviate significantly (residues 74–75, 113–116 and 228–231). In particular, the invisible regions (residues 192–197 and 229–233) in bRIP1 are those that show the largest deviation (Fig. 5*c*). Therefore, the structures of the different liganded forms of bRIP and bRIP$_{SER}$ are all very similar, with the exception of some intrinsically flexible regions (Figs. 5*c* and 5*d*); this is consistent with the results from other RIPs. As shown in other RIP structures, ligand binding does not cause major conformational changes (Gorjanović, 2009; Kurinov *et al.*, 1999; Mak *et al.*, 2007). However, a local adjustment occurs in order to accommodate the adenine moiety of the substrate, accompanied by conformational alteration of the G2 3_{10}-helix (details given below). These conformational

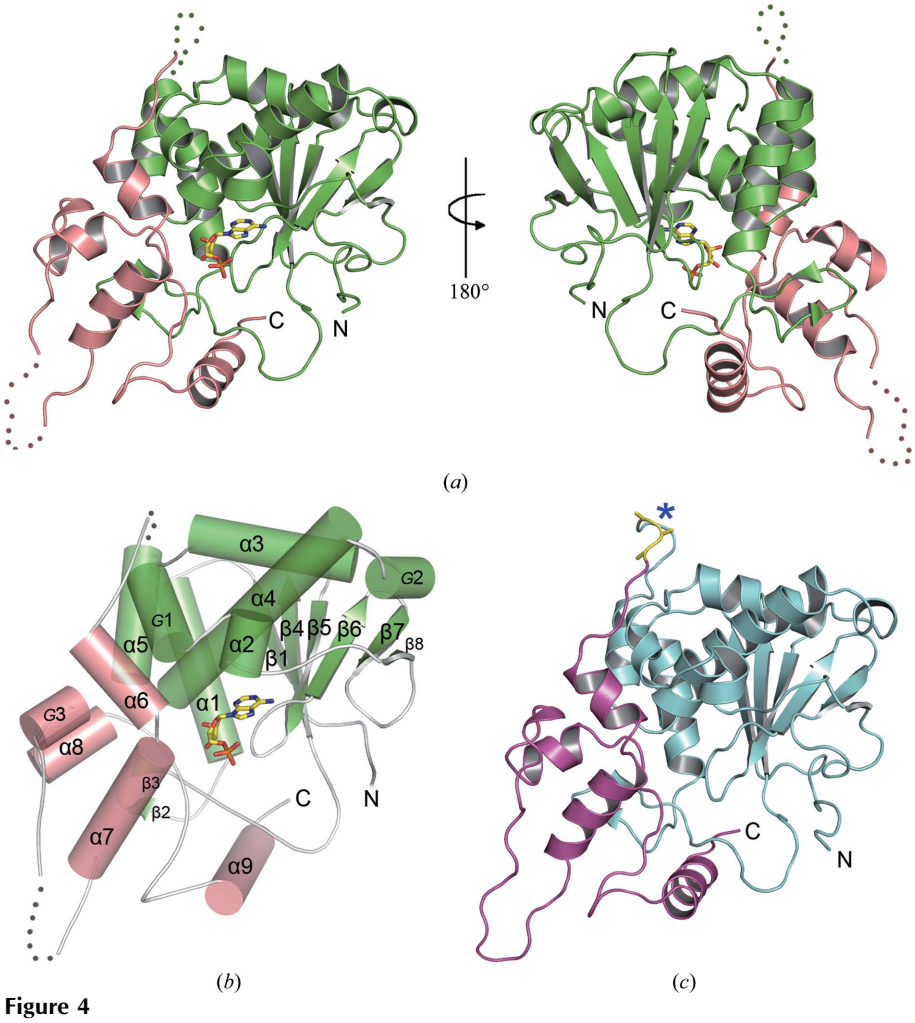

Figure 4
Overall structures of bRIP and bRIP$_{SER}$. (*a*) Front view showing the active site (left) and back view (right) of bRIP. The N-terminal and C-terminal domains are coloured green and salmon pink, respectively. Invisible residues (192–197 and 229–233) are indicated as dots. The AMP in the active site is represented by sticks and the C, N and O atoms are coloured yellow, blue and red, respectively. (*b*) The secondary-structural elements of bRIP are indicated. Helical structures are represented as transparent cylinders. The N- and C-termini are also indicated. (*c*) Structure of one representative chain (D-chain) of bRIP$_{SER}$ from the four molecules present in the asymmetric unit. The N- and C-terminal domains are coloured cyan and purple, respectively. The blue asterisk indicates the SER position (E196A/K197A/K198A; shown as yellow sticks). Invisible regions in bRIP are clearly traced in bRIP$_{SER}$.

differences are observed among all the $bRIP_{SER}$ molecules in the same asymmetric units of the various crystals. Indeed, two different conformations of this region are observed, corresponding to different liganded states, and the electron-density maps for both conformations are very well defined (Figs. 3*a* and 3*b*).

3.5. Structural comparison with other RIPs

The structure of bRIP shows very high similarity to previously determined RIP structures, including charybdin (PDB entry 2b7u; *Z*-score = 27.1, r.m.s.d. = 2.3 Å for 230 matching C^{α} atoms, sequence identity = 28%; Touloupakis *et al.*, 2006), the active form of maize b-32 (PDB entry 2pqi; *Z*-score = 26.2, r.m.s.d. = 2.2 Å for 221 C^{α} atoms, sequence identity = 32%; Mak *et al.*, 2007), the ricin A-chain (PDB entry 2pjo; *Z*-score = 25.4, r.m.s.d. = 2.6 Å for 227 C^{α} atoms, sequence identity = 23%; Carra *et al.*, 2007), PAP (PDB entry 2q8w; *Z*-score = 24.5, r.m.s.d. = 2.1 Å for 219 C^{α} atoms , sequence identity = 21%; T. Hogg, K. Bezouska, N. Ulbrich, I. Kuta Smatanova & R. Hilgenfeld, unpublished work) and trichosanthin (PDB entry 1mrj; *Z*-score = 24.2, r.m.s.d. = 2.4 Å for 218 C^{α} atoms, sequence identity = 19%; Huang *et al.*, 1995). It appears that most of the secondary-structural elements are well superposed. In particular, the structural similarity between bRIP and monocotyledonous RIPs such as charybdin and maize b-32 is higher than that between bRIP and many dicotyledonous RIPs (Figs. 6*a*–6*d*).

Many RIPs share the same protein folding and the residues involved in the active site are structurally conserved, but several differences are also observed. The substrate for the depurinating activity of RIPs is an RNA loop with a specific sequence and the enzymatic specificity differs depending on the RIP. For example, the ricin A-chain and saporin-L1 are distinct in that the former has exquisite specificity for the adenine base within the $GA_{4234}GA$ tetraloop, whereas the latter targets multiple adenines from ribosomes (Endo *et al.*, 1987; Ferreras *et al.*, 1993). Structural studies of ricin and saporin in complex with transition-state analogues indicate different optimal pH values for enzymatic activity and, more importantly, different binding modes of synthetic inhibitors (Sturm *et al.*, 2007) originating from structural differences outside the active site (Ho *et al.*, 2009). Therefore, it is important to analyze the unique structural features of bRIP, whether these are present near the active site or not. Compared with other RIPs, bRIP exhibits significant structural differences in several regions (Fig. 6*a*). There are three unique 3_{10}-helices, G1, G2 and G3, in bRIP; in particular, the G2 helix is markedly different from those observed in other RIPs and shows different conformations within the bRIP structure (Fig. 5*a*). Charybdin has a β-hairpin structure in the equivalent region (Fig. 6*b*), whereas maize b-32 shows a relatively compact structure around this region because several amino-acid residues are deleted (Figs. 6*c* and 6*e*). Comparison with dicotyledonous RIPs such as RTA, TCS and PAP shows more significant differences: a helix (α2) and two long β-strands (β9 and β10) in RTA are absent in the bRIP structure (Figs. 6*d* and 6*e*). The most prominent difference is the extra C-terminal helix α9 (Figs. 6*a* and 6*e*). As shown in Fig. 6(*e*), the other RIPs have much shorter chain lengths and the C-terminal region is not conserved among them. However, RIPs from cereal crops such as barley, wheat and rice show strong sequence conservation in this C-terminal region (Fig. 1). Therefore, we suggest that the unique C-terminal helix α9 might be a structural feature of these RIPs.

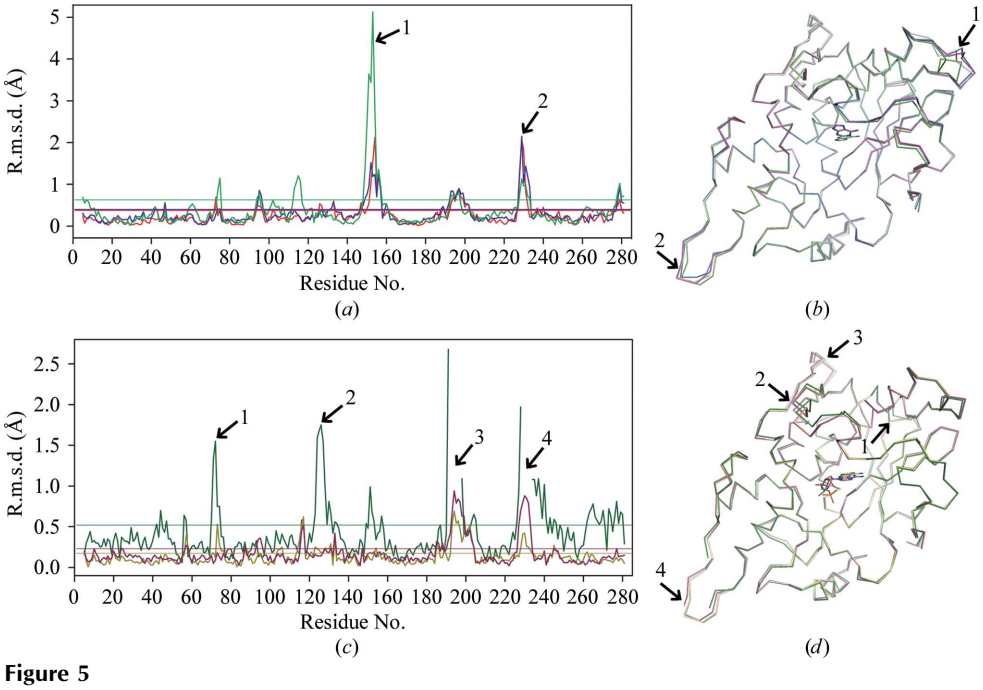

Figure 5
Structural differences among bRIP models. (*a*) Plot of the difference between the C-chain and other chains in the asymmetric unit of adenine-bound $bRIP_{SER}$ (C-chain *versus* A-chain, red line; C-chain *versus* B-chain, blue line; C-chain *versus* D-chain, green line). (*b*) The superposition of C^{α} atoms among chains (A-chain, red; B-chain, blue; C-chain, grey; D-chain, green) in the asymmetric unit of adenine-bound $bRIP_{SER}$. (*c*) Plot of the difference between the D-chain of apo $bRIP_{SER}$ and other models (AMP-bound bRIP, dark green line; D-chain of adenine-bound $bRIP_{SER}$, dark yellow line; D-chain of AMP-bound $bRIP_{SER}$, purple line). (*d*) Superposition of C^{α} atoms among models from different structures (bRIP, green; D-chain of apo $bRIP_{SER}$, grey; D-chain of AMP-bound $bRIP_{SER}$, purple; D-chain of adenine-bound $bRIP_{SER}$, yellow). The r.m.s.d. values for the C^{α} atoms of each residue are plotted as a function of residue number and the horizontal lines indicate the average values for each plot. The regions numbered 1 and 2 in (*a*) and 1, 2, 3 and 4 in (*c*), which are structurally the most variant regions, are indicated in (*b*) and (*d*), respectively.

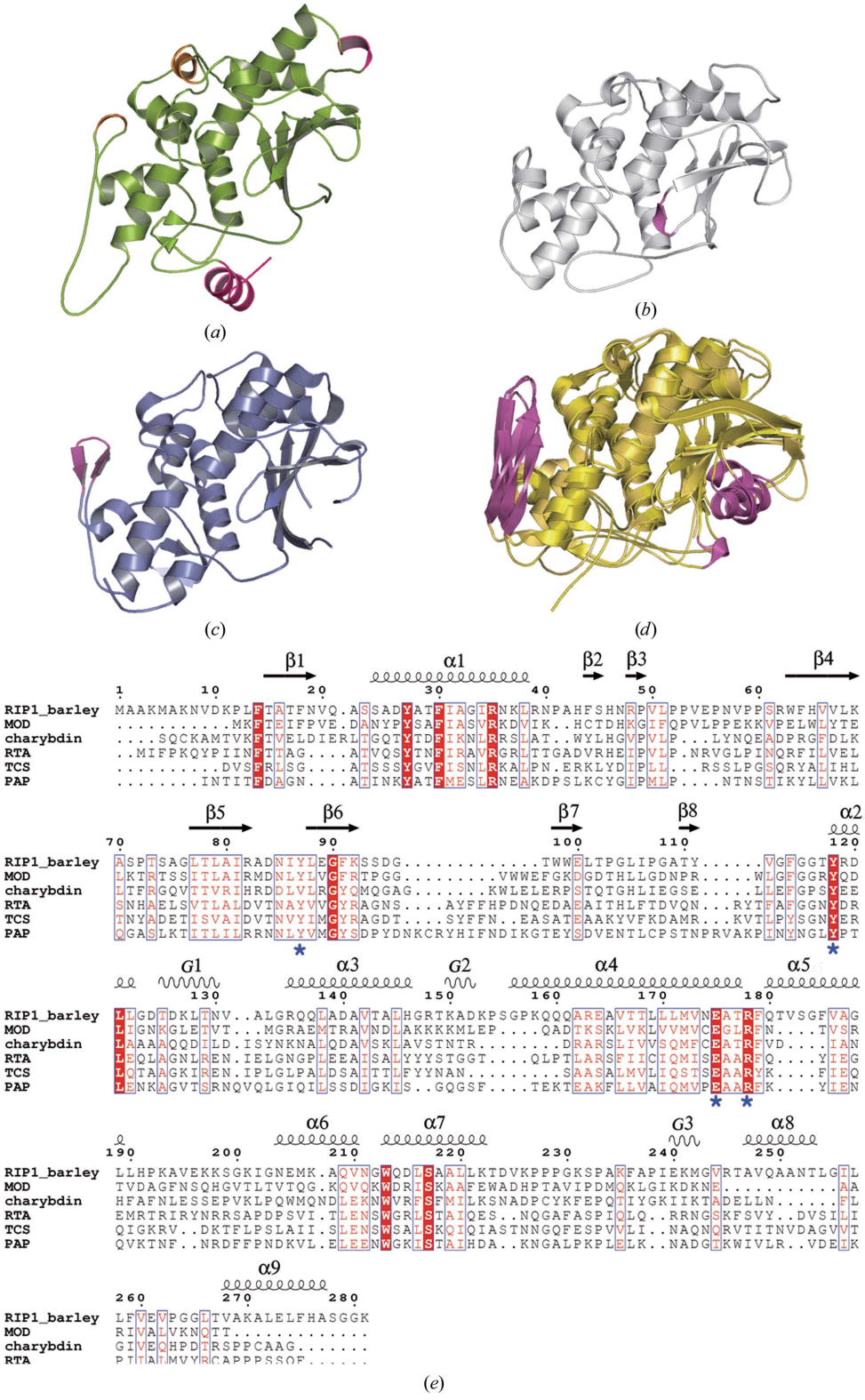

Figure 6
Structural comparison of bRIP with other RIPs. (*a*) Ribbon diagram of bRIP. The unique 3_{10}-helix G2 is coloured purple. The 3_{10}-helices G1 and G3 and the C-terminal helix α9, which are also absent in other RIPs, are coloured orange. (*b–d*) Ribbon representations of other RIPs: (*b*) charybdin (navy; PDB entry 2b7u), (*c*) maize b-32 active form (grey; PDB entry 2pqi) and (*d*) RIPs from dicotyledonous plants, RTA, TCS and PAP (yellow; PDB entries 2pjo, 1mrj and 2p8w, respectively). The regions coloured purple in each RIP (β9–β10 of charybdin; 3_{10}-helix 1 of MOD; α2 and β9–β10 of RTA, TCS and PAP) are absent in bRIP. (*e*) Sequence alignment of bRIP with maize b-32 active form (MOD), charybdin, RTA, TCS and PAP. The catalytic active sites are marked with asterisks.

3.6. Active site

As noted, the N-glycosidase active site is located in a cleft between the larger N-terminal domain and smaller C-terminal domain (Fig. 4*a*). Bound AMP is located in the deep pocket formed by helix α4 and the loops between β5 and β6 and between β8 and α2 of the N-terminal domain; the entrance is partially covered by the adjacent helices α6 and α7 of the C-terminal domain (Fig. 4*a*). The electron density for bound AMP and the surrounding residues is very well defined (Fig. 3*c*). It has been reported that bRIPs, retroviral reverse transcriptases and RNase H share common structural elements, but it has also been suggested that there are important sequence differences among the RIPs (Ready *et al.*, 1988). For example, the RIP from barley seeds has a four-residue insertion (Thr181-Val182-Ser183-Gly184) at the end of the key active-site helix of the ricin A-chain (Ready *et al.*, 1988). We therefore compared the bRIP active site with those in other related structures. However, the four-residue insertion near the active site appears not to have an effect at the structural level because bRIP has a longer helix (α5) located behind the active site (Fig. 6*e*).

A number of the residues participating in the active site, namely Tyr87, Tyr118, Glu175, Arg178 and Trp213, are invariant in the RIP family (Fig. 6*e*; Robertus & Monzingo, 2004). Two charged residues, Glu175 and Arg178 in helix α4, participate in catalysis (Fig. 7*a*). Arg178 makes a salt bridge with Glu175 and forms a hydrogen bond to the carbonyl group of Asn85 in apo bRIP. The Tyr87 in the loop between β5 and β6 and Tyr118 in the loop between β8 and α2 are located on either side of the binding cleft, and the indole ring of Trp213, located between helices α6 and α7, lies parallel to

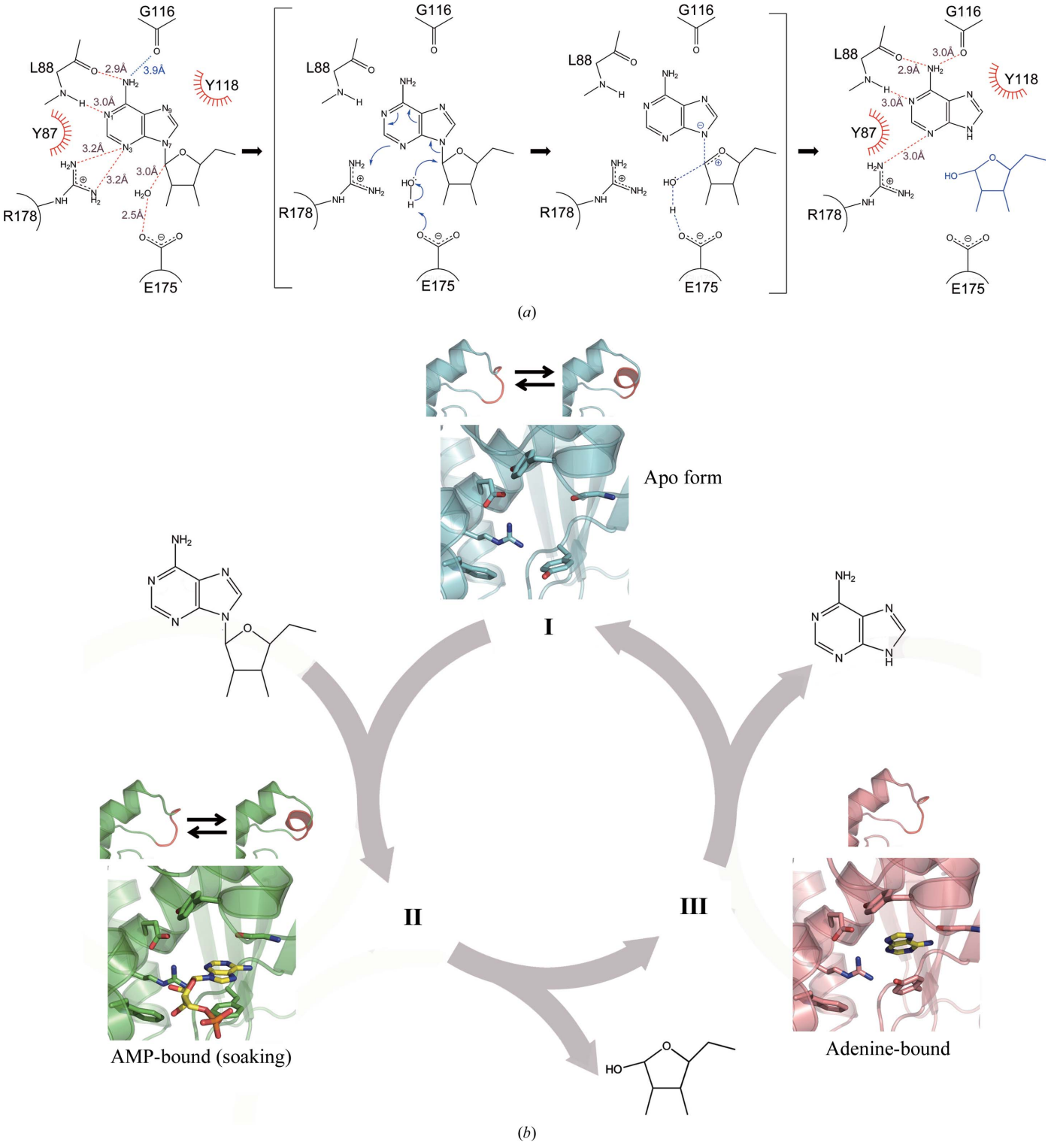

Figure 7
Reaction mechanism and cycle of bRIP. (*a*) A schematic diagram showing the proposed mechanism of N-glycosidic bond hydrolysis by bRIP. Hydrophobic interactions and hydrogen bonds are depicted as red starbursts and dashed lines, respectively. The intermediate states are shown in brackets and the electron flows are indicated as blue arrows. (*b*) A proposed reaction cycle coupled with conformational change at the switch region. Two conformations, 3_{10}-helix and loop, are found in the apo state (I) and in the substrate RNA-bound (AMP in our structure) state (II). Our AMP-bound bRIP structures were obtained by soaking because the electron density observed in the active site of the AMP-cocrystallized bRIP crystal was that of the hydrolyzed product adenine only. Both the apo and AMP-soaked structures possess an open active site to accommodate the incoming substrate. For the hydrolysis of the N-glycosidic bond, Tyr87 needs to be reoriented and bRIP becomes a relatively closed structure, as shown in the adenine-bound structure (III). This is coupled to a conformational change from a loop to a 3_{10}-helix at the switch region. The bound adenine is released and bRIP returns to the apo state. A close-up view showing the details of the active site and the switch region for each enzymatic step is shown. AMP (yellow), Gly116 and the side chains of Tyr87, Tyr118, Glu175, Arg178 and Trp213 are represented by sticks.

Arg178. The most unique feature of the RIP–substrate interaction is the π-stacking between the adenine ring and Tyr87, and Tyr87 might actually be intercalated into the base stacks of the RNA substrate, as in the structures of RIPs complexed with transition-state analogues (Ho *et al.*, 2009). It is known that the π-stacking interaction provides the unique geometry of the RIP–substrate complex; the electron distribution of the adenine ring is very likely to be critical for the stacking interaction. This partially explains why we could not obtain complex crystals of bRIP with an adenine molecule brominated at the 2′- or 8′-position. Although there appears to be no steric hindrance for native complex formation, any electronegative substituent could disturb the π-stacking interaction. Another tyrosine residue at position 118 plays a critical role in the correct orientation of the key glutamate 175. This tyrosine also shows a favourable π-stacking interaction with Arg178, as observed in many other RIP structures. It has been proposed that Glu175 either stabilizes the developing ribocation or acts as a general base with nucleophilic water molecules for the depurination reaction (Robertus & Monzingo, 2004). Recent high-resolution RIP structures with transition-state analogues clearly show that Glu175 acts as general base for activating a water molecule (Ho *et al.*, 2009). We also observed clear electron density for a water molecule at the same position in the AMP-bound bRIP structure (Fig. 3*c*) but not in the adenine-bound and apo bRIP structures. The relative orientation of the adenine moiety is different in different liganded bRIP structures. In particular, the adenine rotates approximately 30° in the adenine-bound bRIP structure compared with the same moiety in the AMP-bound structure (Fig. 7*b*).

3.7. Activation mechanism of bRIP

As noted above, the geometry of the active site of bRIP differs depending on the enzymatic step (Fig. 7*b*). Basically, there are two conformations, 'open' and 'closed', depending on the orientation of Tyr87. A simple explanation for this conformational change is substrate-induced remodelling of the active site of bRIP. However, careful investigation of the structures identified an additional and considerable structural difference in residues 149–153 depending on the different liganded states (Fig. 7*b*) and even different molecules in the asymmetric unit of $bRIP_{SER}$ (Figs. 5*a* and 5*a*). This region actually shows two different conformations: a unique 3_{10}-helix G2 and a loop (Figs. 3*a* and 3*b*). When the G2 helix forms, movement of the loop between the β8 strand and the α2 helix is blocked. Subsequently, this prevents any structural transition from the open to the closed structure to hydrolyze the glycosidic bond. However, the loop region between the β8 strand and the α2 helix is flexible if the G2 segment region exists as a loop and subsequently a local structural adjustment takes place during enzyme catalysis (Fig. 7*b*). Because of this putative regulatory role in catalysis, we defined this region as a 'switch region'. Our bRIP structure is the first RIP structure from a monocotyledonous cereal crop; these plants are highly evolved among the plant kingdom. Moreover, the switch region that we have identified for regulating activity is a unique feature of this RIP subclass. It is very intriguing to compare the structure of this region with those of all known RIP structures. As shown in Fig. 8, type I and type II RIPs from dicotyledonous plants such as the ricin A-chain and PAP show no differences between the apo and the adenine-bound

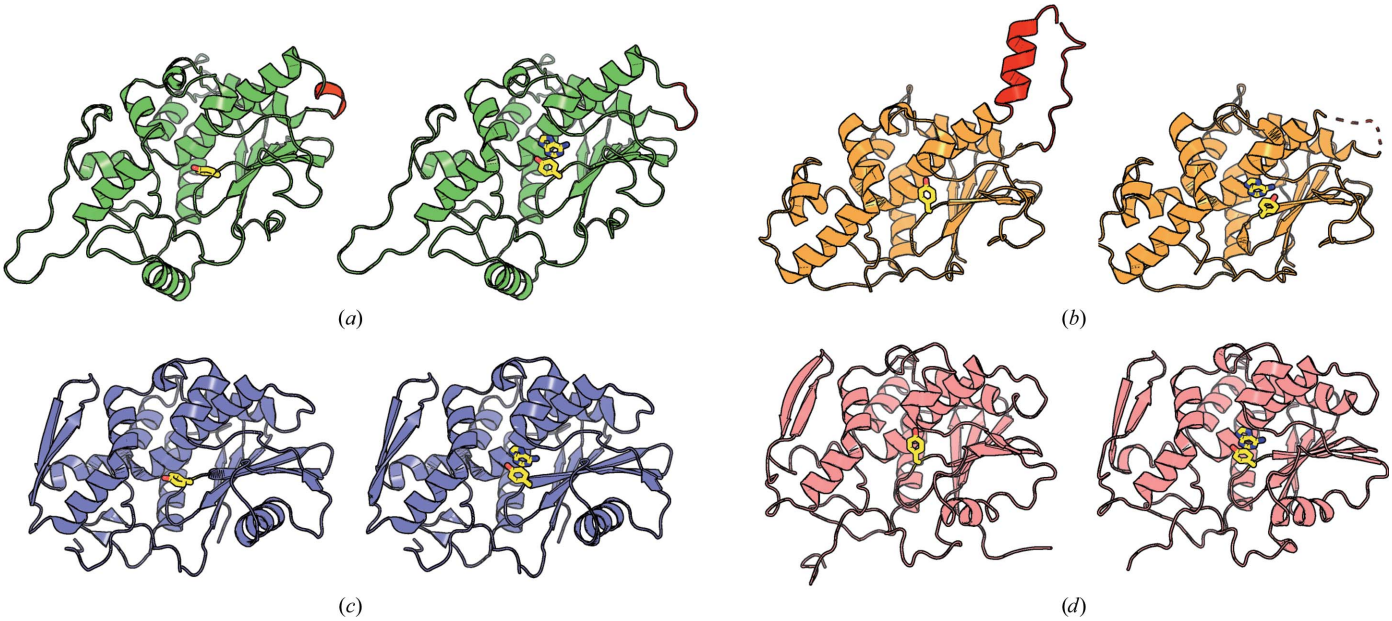

Figure 8
A unique structural feature of bRIP at the switch region. (*a*) A type I RIP (bRIP) from monocots. The green ribbon diagram is of the apo (left) and adenine-bound forms of bRIP (right). The G2 3_{10}-helix or loop is coloured red. (*b*) A type III RIP (maize RIP) from monocots. The orange ribbon diagrams represent inactive (left) and proteolytically cleaved active RIP (right). (*c*) A type I RIP from dicots. The slate-coloured ribbon diagrams represent apo (left) and adenine-bound PAP (right). (*d*) The A-chain of type II RIP from dicots. The pink ribbon diagrams represent the apo (left) and adenine-bound ricin A-chain (right). The key tyrosine residue (Tyr87 in bRIP or equivalent residues in other RIPs) and adenine in each panel are coloured yellow. Notably, there is no conformational change in the 3_{10}-helical region in dicotyledonous RIPs.

structures in the region equivalent to the switch region. However, RIPs from monocotyledonous plants exhibit clear differences. Type III RIP from maize, a monocotyledonous plant, has two distinct states: active and inactive. For the activation of maize RIP (MOD), a specific position of the protruding helical segment has to be cleaved and, interestingly, the proteolytic cleavage site is located at an equivalent position to the switch region of bRIP where the 3_{10}-helix G2 region is situated. Even more intriguingly, this G2 segment region is known as a putative ribosome-binding site in maize RIP (Yang *et al.*, 2010) and some RIPs share the conservation of basic residues in this region that interact with C-terminal ends of ribosomal P proteins for full enzymatic activity (Lapadula *et al.*, 2012). Taken together, we propose that the region near the G2 segment is essential for regulating the N-glycosidase activity in most RIPs, but that each class of RIPs utilizes a different activation mechanism. bRIP, a representative RIP from a monocotyledonous cereal crop, has a flexible conformational transition between a 3_{10}-helix and a loop at the switch region.

4. Conclusions

Crystal structures of barley RIP have been determined in free, AMP-bound and adenine-bound states. For phasing, we attempted to apply several contemporary techniques, as we had obtained the crystal nearly 20 years earlier (Song *et al.*, 1994). bRIP was highly overexpressed as a soluble form in *E. coli* using a synthetic *brip1* gene; therefore, we engineered a useful vector construct (pET-RIP) for heterologous expression. The high-resolution structures defined a catalytic water molecule, key residues in the active site and a conformational switch in the 3_{10}-helix region which is at a position equivalent to that of the proteolytically susceptible site and a putative ribosome-binding site in type III RIP. Our structure confirms the detailed enzymatic mechanism of RIP and reveals a unique activation mechanism for type I RIPs from cereal crops (highly evolved monocotyledonous plants).

We thank the staff at the 17A and NW12 beamlines, the Photon Factory, Japan for help with data collection and thank all of the laboratory members for their helpful advice and discussion, especially S. B. Hong, B.-C. Jeong and S. H. Park for their critical comments on the SER technique and protein expression. This work was supported by a National Research Foundation of Korea (NRF) grant funded by the Korean government (MEST; 2011-0028168) and the Korea Healthcare Technology R&D Project, Ministry for Health, Welfare and Family Affairs, Republic of Korea (A092006). B-GL was supported by a postdoctoral fellowship from the National Research Foundation of Korea (NRF-2011-355-C00049).

References

Adams, P. D. *et al.* (2010). *Acta Cryst.* D**66**, 213–221.
Asano, K., Svensson, B. & Poulsen, F. M. (1984). *Carlsberg Res. Commun.* **49**, 619–626.
Asano, K., Svensson, B., Svendsen, I., Poulsen, F. M. & Roepstorff, P. (1986). *Carlsberg Res. Commun.* **51**, 129–141.
Bieri, S., Potrykus, I. & Fütterer, J. (2000). *Theor. Appl. Genet.* **100**, 755–763.
Bolognesi, A. & Polito, L. (2004). *Mini Rev. Med. Chem.* **4**, 563–583.
Carra, J. H., McHugh, C. A., Mulligan, S., Machiesky, L. M., Soares, A. S. & Millard, C. B. (2007). *BMC Struct. Biol.* **7**, 72.
Chaudhry, B., Müller-Uri, F., Cameron-Mills, V., Gough, S., Simpson, D., Skriver, K. & Mundy, J. (1994). *Plant J.* **6**, 815–824.
Cooper, D. R., Boczek, T., Grelewska, K., Pinkowska, M., Sikorska, M., Zawadzki, M. & Derewenda, Z. (2007). *Acta Cryst.* D**63**, 636–645.
Cowtan, K. (2006). *Acta Cryst.* D**62**, 1002–1011.
Emsley, P., Lohkamp, B., Scott, W. G. & Cowtan, K. (2010). *Acta Cryst.* D**66**, 486–501.
Endo, Y., Mitsui, K., Motizuki, M. & Tsurugi, K. (1987). *J. Biol. Chem.* **262**, 5908–5912.
Endo, Y. & Tsurugi, K. (1987). *J. Biol. Chem.* **262**, 8128–8130.
Endo, Y., Tsurugi, K. & Ebert, R. F. (1988). *Biochim. Biophys. Acta*, **954**, 224–226.
Ferreras, J. M., Barbieri, L., Girbés, T., Battelli, M. G., Rojo, M. A., Arias, F. J., Rocher, M. A., Soriano, F., Mendéz, E. & Stirpe, F. (1993). *Biochim. Biophys. Acta*, **1216**, 31–42.
Goldschmidt, L., Cooper, D. R., Derewenda, Z. S. & Eisenberg, D. (2007). *Protein Sci.* **16**, 1569–1576.
Gorjanović, S. (2009). *J. Inst. Brew.* **115**, 334–360.
Gouet, P., Courcelle, E., Stuart, D. I. & Métoz, F. (1999). *Bioinformatics*, **15**, 305–308.
Gould, J. & Richardson, P. T. (1987). *Oxf. Surv. Plant Mol. Cell. Biol.* **4**, 359–365.
Ho, M. C., Sturm, M. B., Almo, S. C. & Schramm, V. L. (2009). *Proc. Natl Acad. Sci. USA*, **106**, 20276–20281.
Holm, L. & Rosenström, P. (2010). *Nucleic Acids Res.* **38**, W545–W549.
Huang, Q., Liu, S., Tang, Y., Jin, S. & Wang, Y. (1995). *Biochem. J.* **309**, 285–298.
Jeong, Y. J., Jeong, B.-C. & Song, H. K. (2011). *Biochem. Biophys. Res. Commun.* **405**, 112–117.
Kurinov, I. V., Myers, D. E., Irvin, J. D. & Uckun, F. M. (1999). *Protein Sci.* **8**, 1765–1772.
Lapadula, W. J., Sanchez-Puerta, M. V. & Ayub, M. J. (2012). *Toxicon*, **59**, 427–432.
Larkin, M. A., Blackshields, G., Brown, N. P., Chenna, R., McGettigan, P. A., McWilliam, H., Valentin, F., Wallace, I. M., Wilm, A., Lopez, R., Thompson, J. D., Gibson, T. J. & Higgins, D. G. (2007). *Bioinformatics*, **23**, 2947–2948.
Laskowski, R. A., MacArthur, M. W., Moss, D. S. & Thornton, J. M. (1993). *J. Appl. Cryst.* **26**, 283–291.
Leah, R., Tommerup, H., Svendsen, I. & Mundy, J. (1991). *J. Biol. Chem.* **266**, 1564–1573.
Lee-Huang, S., Huang, P. L., Nara, P. L., Chen, H.-C., Kung, H., Huang, P., Huang, H. I. & Huang, P. L. (1990). *FEBS Lett.* **272**, 12–18.
Lodge, J. K., Kaniewski, W. K. & Tumer, N. E. (1993). *Proc. Natl Acad. Sci. USA*, **90**, 7089–7093.
Mak, A. N.-S., Wong, Y.-T., An, Y.-J., Cha, S.-S., Sze, K.-H., Au, S. W.-N., Wong, K.-B. & Shaw, P.-C. (2007). *Nucleic Acids Res.* **35**, 6259–6267.
McCoy, A. J., Grosse-Kunstleve, R. W., Adams, P. D., Winn, M. D., Storoni, L. C. & Read, R. J. (2007). *J. Appl. Cryst.* **40**, 658–674.
McGrath, M. S., Hwang, K. M., Caldwell, S. E., Gaston, I., Luk, K.-C., Wu, P., Ng, V. L., Crowe, S., Daniels, J., Marsh, J., Deinhart, T., Lekas, P. V., Vennari, J. C., Yeung, H.-W. & Lifson, J. D. (1989). *Proc. Natl Acad. Sci. USA*, **86**, 2844–2848.
Mlsna, D., Monzingo, A. F., Katzin, B. J., Ernst, S. & Robertus, J. D. (1993). *Protein Sci.* **2**, 429–435.

Montfort, W., Villafranca, J. E., Monzingo, A. F., Ernst, S. R., Katzin, B., Rutenber, E., Xuong, N. H., Hamlin, R. & Robertus, J. D. (1987). *J. Biol. Chem.* **262**, 5398–5403.
Monzingo, A. F., Collins, E. J., Ernst, S. R., Irvin, J. D. & Robertus, J. D. (1993). *J. Mol. Biol.* **233**, 705–715.
Motto, M. & Lupotto, E. (2004). *Mini Rev. Med. Chem.* **4**, 493–503.
Murshudov, G. N., Skubák, P., Lebedev, A. A., Pannu, N. S., Steiner, R. A., Nicholls, R. A., Winn, M. D., Long, F. & Vagin, A. A. (2011). *Acta Cryst.* D**67**, 355–367.
Nielsen, K. & Boston, R. S. (2001). *Annu. Rev. Plant Physiol. Plant Mol. Biol.* **52**, 785–816.
Otwinowski, Z. & Minor, W. (1997). *Methods Enzymol.* **276**, 307–326.
Parikh, B. A. & Tumer, N. E. (2004). *Mini Rev. Med. Chem.* **4**, 523–543.
Pastan, I. & Kreitman, R. J. (1998). *Adv. Drug Deliv. Rev.* **31**, 53–88.
Peumans, W. J., Hao, Q. & Van Damme, E. J. (2001). *FASEB J.* **15**, 1493–1506.
Polito, L., Bortolotti, M., Pedrazzi, M. & Bolognesi, A. (2011). *Toxins (Basel)*, **3**, 697–720.
Provoda, C. J., Stier, E. M. & Lee, K. D. (2003). *J. Biol. Chem.* **278**, 35102–35108.
Rayment, I. (1997). *Methods Enzymol.* **276**, 171–179.
Ready, M. P., Katzin, B. J. & Robertus, J. D. (1988). *Proteins*, **3**, 53–59.
Roberts, W. K. & Selitrennikoff, C. P. (1986). *Biochim. Biophys. Acta*, **880**, 161–170.
Robertus, J. D. & Monzingo, A. F. (2004). *Mini Rev. Med. Chem.* **4**, 477–486.
Song, H. K., Hwang, K. Y., Kim, K. K. & Suh, S. W. (1994). *Acta Cryst.* D**50**, 910–912.
Stirpe, F. (2004). *Toxicon*, **44**, 371–383.
Stirpe, F., Barbieri, L., Battelli, M. G., Falasca, A. I., Abbondanza, A., Lorenzoni, E. & Stevens, W. A. (1986). *Biochem. J.* **240**, 659–665.
Stirpe, F. & Battelli, M. G. (2006). *Cell. Mol. Life Sci.* **63**, 1850–1866.
Sturm, M. B., Roday, S. & Schramm, V. L. (2007). *J. Am. Chem. Soc.* **129**, 5544–5550.
Tahirov, T. H., Lu, T.-H., Liaw, Y.-C., Chen, Y.-L. & Lin, J.-Y. (1995). *J. Mol. Biol.* **250**, 354–367.
Tillett, D. & Neilan, B. A. (1999). *Nucleic Acids Res.* **27**, e26.
Touloupakis, E., Gessmann, R., Kavelaki, K., Christofakis, E., Petratos, K. & Ghanotakis, D. F. (2006). *FEBS J.* **273**, 2684–2692.
Vagin, A. & Teplyakov, A. (2010). *Acta Cryst.* D**66**, 22–25.
Van Damme, E. J. M., Hao, Q., Chen, Y., Barre, A., Vandenbussche, F., Desmyter, S., Rougé, P. & Peumans, W. J. (2001). *Crit. Rev. Plant Sci.* **20**, 395–465.
Vitetta, E. S. & Uhr, J. W. (1985). *Cell*, **41**, 653–654.
Yang, Y., Mak, A. N.-S., Shaw, P.-C. & Sze, K. H. (2010). *J. Mol. Biol.* **395**, 897–907.
Zhou, K., Fu, Z., Chen, M., Lin, Y. & Pan, K. (1994). *Proteins*, **19**, 4–13.